Showcasing research from Professor Sanjib K. Patra's laboratory, Department of Chemistry, Indian Institute of Technology Kharagpur, Kharagpur, India.
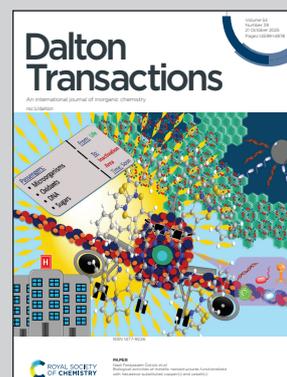
A highly selective Cu^{2+}-coordination triggered multi-stimuli responsive and functional metallogel of bis-terpyridyl-based low molecular weight (LMW) gelator

This work illustrates the successful design of oligo(ethylene glycol)-bridged bis-terpyridyl low molecular weight gelator to achieve Cu(II)-mediated supramolecular gel network. The metallogel manifests intrinsic multistimuli responsiveness and autonomous self-repair, emergent from its dynamic and reversible coordination framework. Beyond structural adaptability, the metallogel operates as a multifunctional soft-material platform, enabling sensing of ammonia, sequestration of anionic dyes such as Congo red, and recyclable catalytic efficacy in the alkyne–azide cycloaddition click reaction, thereby advancing prospects in environmental remediation and sustainable catalytic application.

As featured in:

Dalton Transactions
An international journal of inorganic chemistry
rsc.li/dalton

ROYAL SOCIETY
OF **CHEMISTRY**

rsc.li/dalton

Check for updates

A highly selective Cu²⁺-coordination triggered multi-stimuli responsive and functional metallogel of bis-terpyridyl-based low molecular weight (LMW) gelator

Poulami Panja, [ID] † Utsav Ghosh,† Amit Sil [ID] and Sanjib K. Patra [ID] *

An oligo(ethylene glycol) (OEG) bridged two-armed bis-terpyridyl-based ligand has been synthesized, which can serve as a low molecular weight (LMW) gelator affording a metallogel upon selective coordination to Cu(II) metal ions. The gelator can form a metallogel at a concentration as low as 0.5 wt%. The gel exhibits various remarkable stimuli responsive behaviors with an alternate gel to sol transition, and it responds to a wide range of stimuli, including pH, temperature, and mechanical and chemical stimuli. The obtained soft material has been fully characterized by using a combination of experimental techniques, including scanning electron microscopy (SEM), transmission electron microscopy (TEM), and rheology measurements. The metallogel exhibits multifunctional properties, including self-healing behavior, and can tolerate a wide range of physical and chemical changes. The gel in its dried form (xerogel) shows excellent selective adsorption properties towards the anionic dye Congo red. Moreover, the gel can also detect ammonia in the gel state by changing color and state. Most importantly, the fibrous networked metallogel also exhibits excellent catalytic activity for the azide–alkyne cycloaddition (CuAAC) reaction and serves as a recyclable catalyst supported by the air-stable networked xerogel.

1. Introduction

The structural diversity and multifunctionality observed within biological macromolecules has attracted tremendous interest in investigating hierarchical self-assembly for generating supramolecular assemblies where both the properties and performance can be governed and tuned by weak non-covalent interactions.[1,2] Amongst various self-assembled soft materials, supramolecular gels have emerged as smart and multifunctional materials with versatile potential applications of academic and industrial interest, including drug delivery,[3–7] catalytic studies,[8] electrochemical devices, optoelectronic devices,[9,10] light-harvesting materials,[11,12] tissue engineering, nanoscience and nanotechnologies.[13,14] Unlike the conventional supramolecular polymeric network (SPN) consisting of a giant structure formed by covalent interactions, low molecular weight (LMW) gelators form a novel class of supramolecular materials following a 'bottom-up' strategy through non-covalent interactions.[15–21] The supramolecular self-assembly of small molecules represents a powerful strategy for the con-

struction of nanostructured materials, among which supramolecular gels with liquid flow and solid plastic characteristics often exhibit reversible phase transitions due to the presence of weak intermolecular non-covalent interactions, such as dispersion forces, hydrogen bonding, and π–π and electrostatic interactions.[22–24] The self-healing property of low molecular weight gels is extremely important in the field of biomaterial preparation and also in tissue engineering.[25] More interestingly and importantly, the relatively weak nature of non-covalent interactions can lead to a reversible sol–gel transition modulated by a range of stimuli, such as temperature, pH and light, showing versatility in stimuli-responsive materials.[26–31]

Dried solid xerogels also possess the unique characteristic of the removal of toxic adulterants in the environment, like organic dyes. Many of these dyes are very stable and non-biodegradable, causing environmental and health hazards. They are resistant to aerobic digestion and represent one of the difficult categories of pollutants to be removed from industrial wastewater. These dyes, being highly toxic and even carcinogenic to microbial populations and mammalian animals, need to be removed from water effluents before they are released into water bodies.[32,33] Due to the environmental and health concerns associated with wastewater effluents, different separation techniques have been used in the removal of dyes from aqueous solutions.[34] The development of various physical,

Department of Chemistry, Indian Institute of Technology Kharagpur, Kharagpur 721302, WB, India. E-mail: skpatra@chem.iitkgp.ac.in; Tel: +913222283338
† These authors contributed equally to this work and share first authorship.

chemical and biological methodologies, such as coagulation, adsorption and advance chemical oxidation, has emerged as a solution to remove dyes from water.[35] Out of the numerous types of adsorbents available now-a-days, xerogels are one of the efficient materials that offer a cost-effective and recyclable route for waste water treatment by adsorbing toxic dyes from water bodies. Hence, recently, there has been considerable effort towards using metallogels as adsorption materials for application in environmental remediation.[36–39]

In another direction, there has been exceptional effort towards the development of gel materials for application as sustainable catalysts.[40–44] Compared to polymer gels, low molecular weight gels, due to their well-defined mode of self-assembly, could be considered as a major candidate for potential function in catalysis. Such highly organized self-assembly process could control the orientation of existing reactive or catalytic groups and bring them into a critical proximity, which in principle could have an impact on the reactivity in comparison with homogeneous phase or less structured polymer-based gels.[45] The incorporation of catalytically active metal ions into metallogels offers the opportunity to develop a novel class of reusable heterogeneous sustainable catalysts. Moreover, the scope of controlling the surface area, pore volume, and average pore diameter further make self-assembled gels attractive candidates for catalytic applications.

The diverse nature of the metal–organic network can immobilize a voluminous number of solvent molecules, giving rising to different classes of gelling materials.[46,47] Amongst them, metal ion coordination driven self-assembly forms a novel class of supramolecular metallogels where the additionally existing metal–metal interactions and metal–ligand interactions together with the hydrogen bonding interactions, hydrophobic interactions and aromatic π–π stacking interactions account for their stability to form self-assembled functional nano- or micro-structures.[48–53] In comparison with organogels, relatively less-explored metallogels exhibit intriguing "smart" properties since the incorporation of metal (alkaline earth, transition, late transition and lanthanides) ions into gelator molecules transmits the metal characteristics, such as conductive, redox, magnetic, catalytic or luminescent properties, into the gel, thus providing additional subtle control over the molecular assembly.[54–58] The emerging properties stemming from the metal ion most often include redox active properties, catalytic properties and magnetic properties, and thus several researchers have given significant attention to the development of functional gel materials based on these low molecular weight gelators (LMWGs) over the last few decades.[59–66] The formation of metallogels typically follows two main strategies: (i) the self-assembly of discrete metal complexes *via* non-covalent interactions such as hydrogen bonding, π–π stacking, and metal–metal interactions, enabling them to act as gelators; or (ii) coordination-driven assembly, where metal–ligand interactions give rise to highly cross-linked, polymer-like networks capable of entrapping large volumes of solvent within the gel matrix.

It is well-known that oligo(ethylene glycol) moieties are capable of forming hydrogen bonds, and they have been widely used as building blocks to create a variety of molecularly assembled structures and gels with a wide range of solvents at a very low concentration.[67] The terpyridyl-based system is one of the most extensively studied families of N-donor chelating ligands forming stable complexes with a wide range of metal ions, and may serve as a building block for metal-containing supramolecular systems.[68–78] Recently, it has been demonstrated that the perfluoroalkylamide derivative of 4-aminophenyl-2,2′,6,2′-terpyridine spontaneously self-assembles into gels, which exhibit an unprecedented rapid gel strength recovery and thermal rearrangement in aqueous dimethyl sulfoxide.[79] These gels were shown to exhibit multiple stimuli-responsive behaviors, including thermo-, chemo-, and mechanical responses.

In this present work, a low molecular weight gelator based on oligo(ethylene glycol) bridged bis-terpyridyl to access metallogels has been developed. The gelator forms stable and multi-functional metallogels selectively in the presence of copper(II) ions (irrespective of the anions). Therefore, the functionalization of the oligo(ethylene glycol) moiety with a terpyridyl group provides a straightforward strategy for the formation of low molecular weight metallogels featuring metal ion-ligand coordination complexes. The gel responds to dynamic pH and temperature variations and could be interesting for biomedical applications. The produced metallogel possesses self-healing properties along with self-sustainability and can tolerate a wide range of physical and chemical changes. The synthesized dried metallogel (xerogel) displays adsorbing properties towards a specific dye (Congo red) in aqueous medium. Most importantly and interestingly, the metallogel also exhibits promising catalytic properties towards click reactions.

2. Results and discussion

Design and synthesis of the LMW gelator

Aiming to access metallogels, a small molecular weight gelator was first tailored with potential interaction sites. To facilitate the formation of metallogels by using non-covalent and metal–ligand interactions, we synthesized a two-armed bis-terpyridyl ligand with an oligo(ethylene glycol) bridge, which can undergo complexation with a Cu(II) metal centre both in aqueous and organic solvents. Its extended π-conjugation and planarity further promote supramolecular ordering and gelation *via* π–π stacking and metal–ligand cross-linking, essential for metallogel formation. The ligand was designed with all the essential functional groups required for gelation, such as hydrogen bonding sites as well as π–π stacking and metal–ligand interactions.[80] The synthetic scheme of our designed bis-terpyridyl-based gelator (**L1**) is outlined in Scheme 1, involving a stepwise approach starting from 4′-(4-methylphenyl)-2,2′:6′,2″-terpyridine (**1**), which was synthesized following the Kröhnke method involving condensation of 4-methylbenzaldehyde with 2-acetyl pyridine.[81] NBS-mediated benzylic bromination of **1** with a catalytic amount of 2,2′-azobisisobutyronitrile (AIBN) yielded **2**, which was confirmed from NMR spectroscopy and mass spectrometry
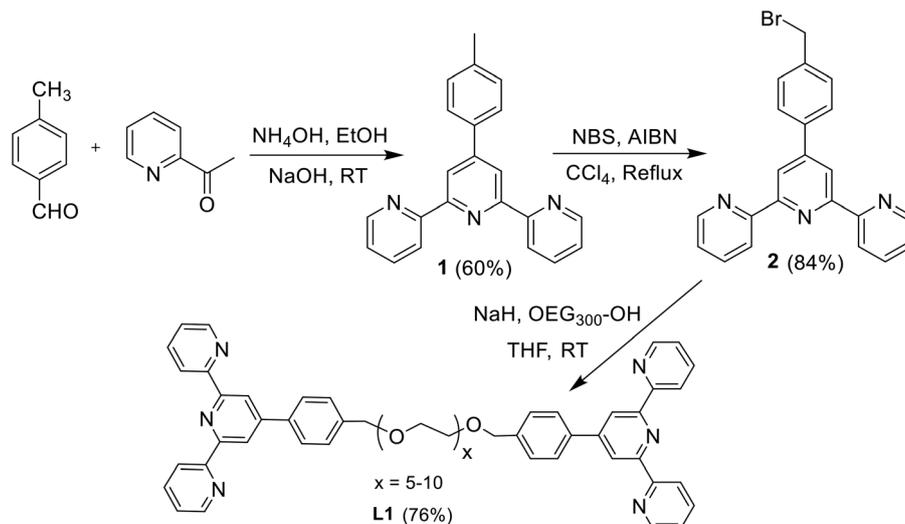
Scheme 1 Synthetic scheme for the low molecular weight gelator **L1**.

(Fig. S1–S6, S10 and S11).[82] The dropwise addition of a solution of **2** to a solution of oligo(ethylene glycol) (OEG$_{300}$) and sodium hydride followed by extraction from ethyl acetate furnished the gelator **L1**.[83] The bis-terpyridyl compound **L1** was characterized unambiguously by ^1H, ^{13}C and mass spectrometry. In ^1H NMR, the signals for the aromatic protons are observed in the range of 7.34–8.34 ppm. The benzylic protons resonate at 4.66 ppm, whereas the protons of the OEG$_{300}$ moiety resonate in the region of 3.64–3.71 ppm. In ^{13}C NMR, the carbons of OEG and aromatic moieties appeared at 69.1–72.8 ppm and 118.6–156.2, respectively (Fig. S7 and S8). The MALDI-TOF study further confirms the chemical structure by showing the peaks for the corresponding different numbers of "–CH$_2$CH$_2$O–" units in the OEG moiety as expected (Fig. S12).

Gelation studies

The gelation ability of the low molecular weight gelator, **L1**, was assessed by mixing a methanolic solution of it and a series of various metal salts ranging from alkaline earth metal to transition metal ions (MCl$_2$ salts: M = Mg, Ca, Mn, Fe, Co, Ni, Cu, Zn, Cd, Hg; MCl$_3$: FeCl$_3$) in aqueous solution with an equimolar ratio at 50 °C in a systematic way, followed by the slow cooling of the mixture to 28 °C (ambient temperature).

Initially, the resulting solution either formed a transparent green coloured solution or generated precipitation of the resulting complexes even after keeping it for 12 h. To our surprise, when we added 2 N HCl to reach a pH around 2 (as confirmed by pH paper), **L1** was found to undergo greenish coloured metallogel (**MG1**) formation instantly within 5 min in the presence of Cu(II) selectively as shown in Fig. 1, and Fig. S14. A schematic illustration of the metallogel formation process is presented in Fig. 2a. The gelator concentration was then varied while keeping the metal ion concentration fixed. It was observed that mixing the two solutions at different **L1**/Cu(II) ratios can give translucent metallogels, which led us to conclude that in spite of the relatively low molar concentration of the metal ion, following a similar condition would eventually give rise to metallogel formation (Fig. 2b). The metallogel was pH sensitive and stable in the range of pH 1 to 3. The propensity of the gelation ability in each case was confirmed by resistance to flow upon inversion of the screw-capped vials. To investigate the role of anions in the Cu^{2+}-coordination gel formation, various Cu(II) salts were chosen with different counter anions employing chloride, nitrate and sulphate. While maintaining all the necessary conditions for gel formation, each of them resulted in strong gel formation. From here, it can be
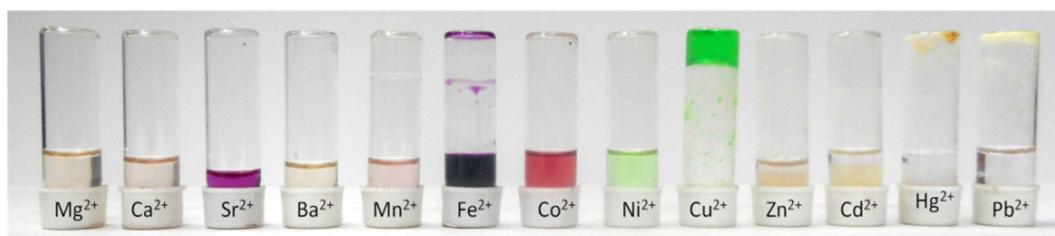

Fig. 1 Demonstration of metallogel (**MG1**) formation with 6 mM **L1** and 6 mM concentrations of various metal salts in MeOH, showing selectivity towards Cu(II) only (pH was maintained at ~2).
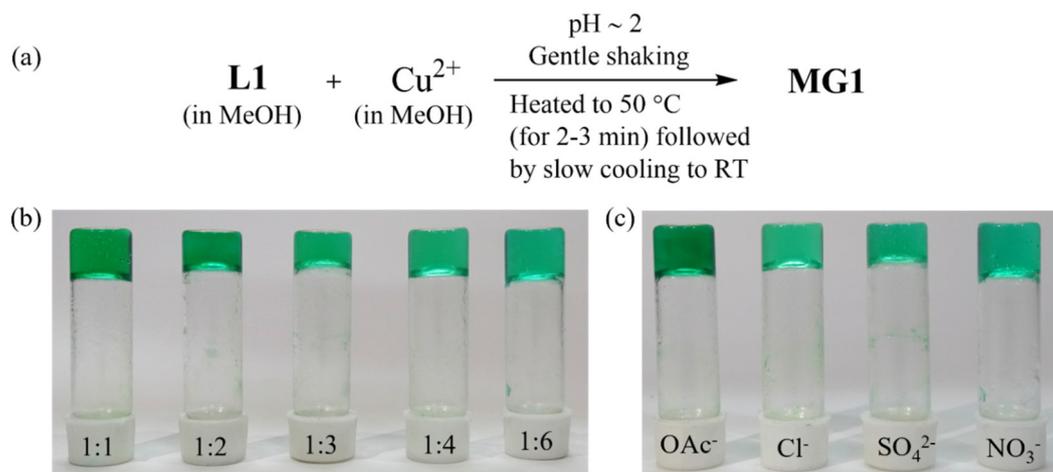
Fig. 2 (a) A schematic presentation of the metallogelation process. (b) Gelation observed at various Cu(II) ion : gelator ratios. Cu(II)-acetate in MeOH was used for gelation. (c) A demonstration of anion independence in the gelation of **L1** with different Cu(II) salts. pH was maintained at ~2 in all cases.

concluded that the choice of the anion is completely independent of the gel formation, as the counter anions have no visible influence on Cu(II)-metallogel formation (Fig. 2c).

To further understand the role of the solvents in metallogel formation, a wide range of polar and nonpolar solvents, including MeOH, DMF, DMSO, H_2O, $CHCl_3$, DCM, THF, hexanes and toluene, were checked. Except in DMF, DMSO, MeOH and H_2O, gelation was not observed, resulting in precipitate formation (Fig. S15). The consolidated results, and temporal evolution of gel formation are detailed in Table S1. In each of the cases, the state of the gel material was tested by the conventional "stable-upon-inversion of the vial" method. Interestingly, it was observed that **L1** could undergo gel formation instantly with a gelator concentration as low as 0.5 wt% (w/v) in solvents such as DMF, DMSO, MeOH and H_2O in the presence of Cu(II) at pH around 2 under similar conditions. Most importantly, treating an aqueous solution of copper(II) acetate and **L1** (6 mmol) yielded translucent metallogels for different **L1**/Cu(II) ratios.

The absorption spectrum of the gelator **L1** in dry DCM solvent shows a characteristic band centred at 280 nm, due to the π–π* transition of the terpyridyl ligand (Fig. S17a). The UV-Vis absorption spectrum of the metallogel was then acquired by placing the sample on a cover slip and covering it with a second slip to ensure proper placement during measurement. In the case of the metallogel, the band shifted to 320 nm (λ_{max}) along with a broad shoulder at around 360 nm, which is presumably due to the n–π* and π–π* transitions associated with the terpyridyl ligands.[84] A very weak and broad absorption band was observed in the range of 480–520 nm that originated from the Laporte-forbidden spin-allowed d–d transitions for the Cu(II) centre. Due to the low molar absorptivity ($\varepsilon < 100\ M^{-1}\ cm^{-1}$), this band remains unresolved in the metallogel state.[85,86] An increase in the extent of aggregation corresponds to a more pronounced broadening of

the shoulder, reflecting enhanced intermolecular interactions and ordered assembly.[87]

Stimuli-responsive behavior and sol–gel transition of the Cu(II)-metallogel

During the fabrication of metallo-supramolecular assemblies, the strategic selection of metal ions plays a pivotal role in imparting distinct functional advantages to the resulting materials. In our system also, the coordination of ligands with Cu(II) ions selectively induces metallogel formation and imparts distinctive multi-responsive properties to the resulting material (Fig. 3 and Fig. S16). Notably, thermal stimulus induces a reversible sol–gel transition, wherein the gel undergoes liquefaction upon heating, while its structural integrity is spontaneously restored upon cooling to ambient temperature, thereby substantiating its thermo-responsive nature. The kinetics of gel recovery are intrinsically dependent on ligand concentration, typically occurring within a time frame of 5 to 10 minutes. Furthermore, an additional characteristic of considerable interest is the mechano-responsive behavior exhibited by the metallogel. Upon the application of external mechanical perturbations, such as vigorous agitation or sonication, the gel is transformed to a free-flowing liquid state. However, upon cessation of the applied force, the system undergoes spontaneous self-reorganization, culminating in the reformation of a green translucent gel (Fig. 3). This phenomenon underscores the dynamic reversibility of the sol–gel transition, which persists even under prolonged sonication, highlighting the robustness and adaptive nature of the system.

An investigation into the chemical stimulus-responsiveness of this metallogel was also subsequently undertaken, with a particular focus on evaluating the effect of exceptionally strong chelating agent EDTA on the metallogel incorporating Cu(II) ions. As depicted in Fig. 3, the introduction of one equivalent (per Cu^{2+}) of solid EDTA disodium salt at 25 °C resulted in the
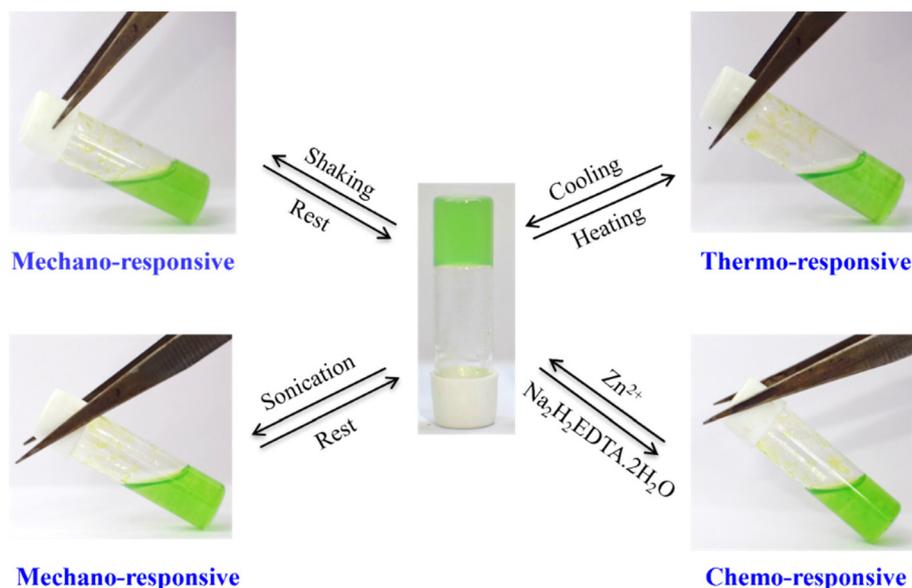
Fig. 3 An illustrative pictorial representation of the multi-stimuli responsive behavior of **MG1** (metallogel prepared with 6 mM **L1** and 6 mM Cu(II)-acetate in MeOH).

gradual formation of a transparent solution that retained its green color without any noticeable change in hue. This transformation signifies the disintegration of the gel matrix, as EDTA exhibits a markedly higher chelating affinity for Cu(II) ions than the **L1** ligand itself. Consequently, this disruption emphasizes the essential role of **L1**-Cu(II) complexation in facilitating and sustaining gel formation. Furthermore, the reversibility of this transition was substantiated through the sequential introduction of Zn^{2+} ions (as $Zn(OAc)_2 \cdot 2H_2O$) in a 1.5-fold molar excess relative to the EDTA concentration. Upon addition of this Zn(II) salt to the EDTA-induced solubilized system, a rapid gelation process was observed, with the solution reverting to its gel state upon brief agitation. The UV-vis spectrum of the **MG1** sample after treatment with EDTA closely resembles the spectrum of the free ligand (**L1**), indicating the disruption of the metal–ligand interactions and reversible coordination process (Fig. S17b). These findings elucidate the dynamic and reversible nature of the macroscopic gel–sol transition within the Cu(II)-induced metallogel, wherein the modulation of the EDTA concentration serves as a precise chemical trigger. Moreover, the cyclic addition of EDTA and Cu(II) ions facilitated repeated oscillations between the sol and gel phases, further corroborating the reversible nature of this transition and emphasizing the stimuli-responsive characteristics of the metallogel system.

Another remarkable manifestation of the chemo-responsive nature of the metallogel is its ability to undergo structural disintegration upon exposure to aqueous ammonia (NH_3) within the gel matrix. The presence of ammonia induces a striking visual change, wherein the characteristic green gel transitions into a deep-blue sol, signifying alterations in the coordination environment of the copper(II) ion disrupting the gel network, culminating in the formation of a blue sol of tetraaminecop-

per(II) complex (Fig. 4). This distinct transition highlights the metallogel's exceptional aptitude as a chemosensor, capable of detecting ammonia by the Cu(II)-metallogel. Furthermore, upon exposure to hydrochloric acid (HCl), the ammonia-coordinated Cu(II) sol undergoes a complete reversion to its original state, demonstrating the reversibility of this sol–gel transition. Notably, this cyclic transformation between the sol and gel phases, driven by modulating the pH of the medium, can be iterated multiple times without compromising the critical gelator concentration. This dynamic equilibrium, governed by the dissociation and reformation of coordination bonds between the metal ion and gelator molecules, underscores the intricate molecular interplay that governs the structural adaptability of the metallogel system.

Morphology studies

To gain deeper insights into the intricate nucleation dynamics and propagation mechanisms underlying self-assembly in diverse conditions, the morphological characteristics of the gel were examined through scanning electron microscopy (SEM) and transmission electron microscopy (TEM) techniques. Field-emission scanning electron microscopy (FESEM) analysis provided a comprehensive exploration of the microstructural patterns inherent to the metallogel, elucidating its supramolecular framework, leading to stable Cu(II)-based supramolecular metallogels (Fig. 5a and b). The FESEM micrographs of other Cu^{2+}-metallogels distinctly reveal the presence of an intricate fibrillar network, indicative of a highly interconnected supramolecular architecture (Fig. S18a–d). Furthermore, elemental mapping analysis confirmed the presence of essential elements, especially copper, confirming the composition of the metallogel (Fig. S19 and S20). Notably, the xerogel morphology exhibited in the dried state showed a change from
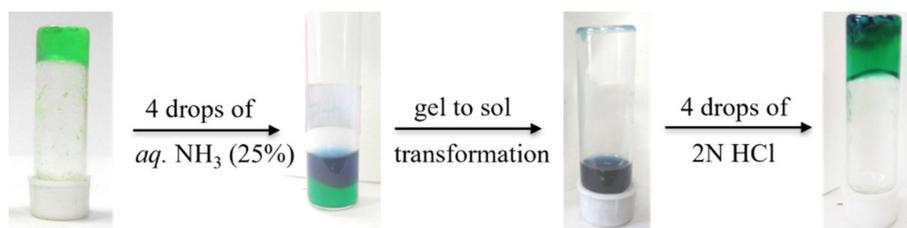
Fig. 4 The reversible gel–sol transition induced by aqueous ammonia and its restoration *via* acidic modulation by the addition of dilute HCl.
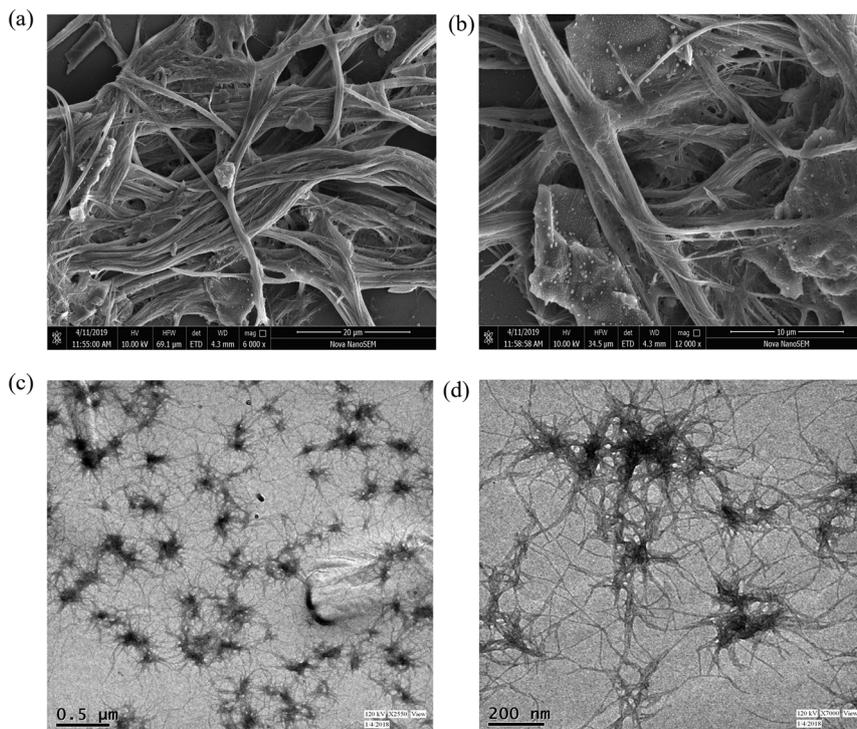

Fig. 5 FESEM images of **MG1** in a 1 : 1 Cu(II)-acetate/**L1** ratio showing a fibrillary network. Scale: (a) 20 µm, (b) 10 µm; TEM images (bright field) of **MG1** in a 1 : 1 Cu(II)-acetate/**L1** ratio. Scale: (c) 0.5 µm, (d) 200 nm.

that of the freshly prepared metallogel, highlighting the impact of solvent removal on the material's morphology (Fig. S21 and 22). Additionally, TEM imaging further substantiated the fibrous network characteristic of the metallogels, providing microscopic evidence of the hierarchical self-assembled architectures (Fig. 5c, d and Fig. S23a–h). Furthermore, elemental mapping was performed using STEM analysis, as shown in Fig. S24, revealing the spatial distribution of the constituent elements and confirming the uniform incorporation of metal ions throughout the gel matrix.

Rheology studies

To investigate the mechanical properties of the metallogel, rheological studies have been carried out through angular frequency and strain sweep measurement. In order to under-

stand the thixotropic behavior of the Cu(II)-based gel (**MG1**), the corresponding properties have been extensively studied in three different solvent systems (methanol, DMSO, DMF) in detail. The amount of energy held in the system during the application of shear on the viscoelastic area is represented by the storage modulus (G'). The amount of energy lost when oscillatory tension is applied is represented by the loss modulus (G''). The value of G' is considerably higher in the gel state at *ca.* 1000 Pa for methanol (Fig. 6a), indicating a gel of moderate strength compared to the metallogel formed in other solvents (Fig. 6b and c). The viscoelastic properties of the metallogel were comparable to those commonly seen for a crosslinked polymer system.[88] At first, the linear viscoelastic region was chosen and the storage modulus and loss modulus values were measured as functions of shear stress at a constant frequency of 1 rad s^{-1} and at a constant temperature of
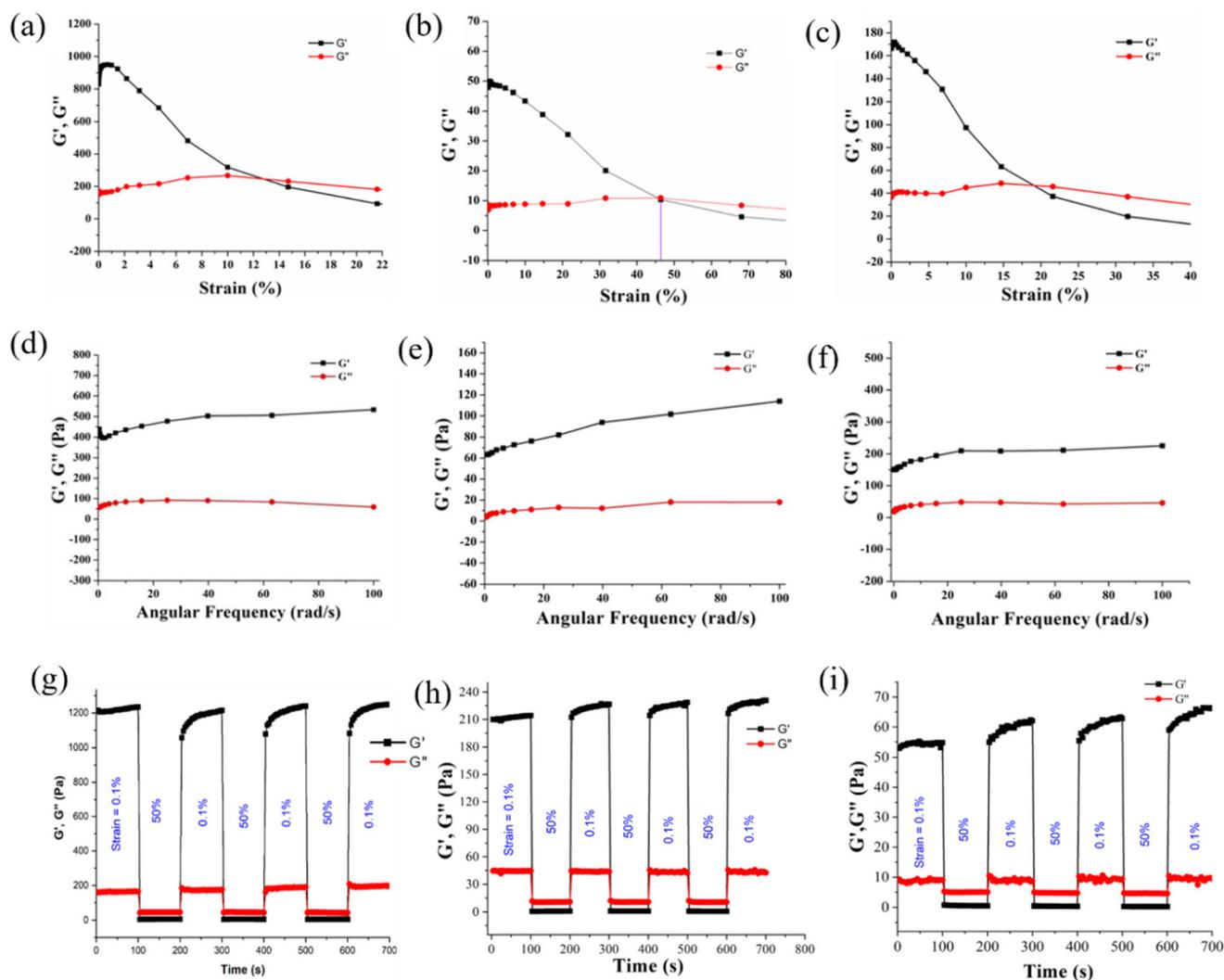
Fig. 6 Variation of storage modulus (G') and loss modulus (G'') for **MG1** formed in (a) methanol, (b) DMSO and (c) DMF as a function of strain amplitude (at a frequency of 1 rad s^{-1}); variation of the storage modulus (G') and loss modulus (G'') for the metallogel formed in (d) methanol, (e) DMSO and (f) DMF as a function of angular frequency (at 1 rad s^{-1}). All the gels were prepared with 1 : 1 Cu(II)-acetate/gelator. Step strain experiment of **MG1** in various solvents: (g) methanol, (h) DMSO and (i) DMF, recorded at a frequency of 10 rad s^{-1}.

25 °C. At low strain amplitudes, the response was solid-like where the storage modulus (G') remained higher than that of the loss moduli constant (G''). At the higher frequency region when the yield strain was increased, it reached a point where the gel started to flow and G' decreased, indicating a crossover region. A gradual increase in shear strain value up to 13%, however, resulted in complete reversal of the magnitudes in G' and G'', exhibiting the loss of the viscoelastic nature of the gel material. The metallogel **MG1**, however, shows a reversible mechano-responsive gel–sol transition behaviour when the shear strain amplitude is decreased. The dynamic properties of the metallogels were then investigated in the linear viscoelastic regime by frequency sweep measurements. The angular frequency sweep data are shown in Fig. 6d–f. In the investigated frequency range, the elastic moduli were constant and about a few orders of magnitude higher than the loss moduli

at different concentrations. The slightly increasing values of G' and G'' along with the steadily increasing frequency suggested that the energy storage process occurred without obvious energy dissipation during the test. The increased gap between the G' and G'' indicated that the metallogels have better viscid properties than elasticity. To confirm the viscoelastic nature, we performed a step-strain experiment with **MG1** at 25 °C (Fig. 6g–i). The experiment was carried out in a methanol environment to avoid the evaporation of methanol. In the first step, a constant strain of 0.1% was applied and then the strain was increased to 50% to break the gel. Then after a few minutes, the strain was decreased from 50% to 0.1% and kept for a few minutes to reform the gel. During these consecutive cycles of applying low and high strain at a time interval, the **MG1** converts gel-to-sol ($G' < G''$) and *vice versa* ($G' > G''$). After every cycle of breaking and reformation

of the gel, the recovery of the gel state was almost 100% in the step-strain experiment.

It has been reported that the metallogels could stand by themselves without any support and without changing their shape due to their self-sustaining nature.[89,90] To demonstrate the self-sustaining nature of the metallogels, they were fabricated in a 10 mL syringe (cylindrical tube of 1 cm diameter) and brought out carefully. The metallogels retained their initial shape as formed inside the syringe tube. But among all, the metallogel prepared in MeOH exhibits the best self-sustaining behavior. Using the free-standing gel blocks of **MG1** (gelator/metal ion ratio of 1 : 1), we can make different shapes of gel, such as a cylinder or rectangle. The self-sustaining nature indicates that the metallogels with immobilized solvent molecules are very stable and intact. The metallogel also exhibits remarkable load-bearing capacity, as demonstrated in Fig. 7, where the cylindrical shaped **MG1** is examined to demonstrate its rigidity by incrementally placing Indian 5-rupee coins (each weighing approximately 5 g) onto the gel surface. It was found that the gel cylinder can take a load of 9 coins (*ca.* 45 g) with *ca.* 50% reduction in the height of the gel sample. The height of the **MG1** reduces due to the partial release of immobilized MeOH from the gel as the load increases. Such a load bearing capacity is exceptional for a low molecular weight gelator with limited reports.[91]

Self-healing behavior

The self-healing capability of metallogels is fundamentally characterized by their intrinsic ability to autonomously re-establish disrupted bonding interactions following mechanical damage, closely mimicking the regenerative behavior observed in biological tissues.[92] Given their immense potential in biomaterials and tissue engineering, the development of novel self-healing metallogels has garnered significant scientific interest.[28,30,31] These advanced materials exhibit a dynamic

and reversible network, enabling them to restore their structural integrity without external intervention. The metallogel **MG1**, in particular, exhibited notable adhesive characteristics, as evidenced by its ability to seamlessly reattach severed sections upon brief physical contact, wherein the cut pieces adhered effectively after being allowed to remain in proximity for a few minutes as demonstrated in Fig. 8. This intrinsic stickiness further reinforces its potential in soft material engineering, biomedical applications, and smart material design, where self-repairing and adhesive properties are highly desirable. Furthermore, **MG1** demonstrated exceptional malleability and self-repairing properties, allowing it to be molded into various structural configurations, while retaining its ability to autonomously reform and heal. This remarkable adaptability underscores its suitability for applications requiring mechanical robustness and dynamic responsiveness.

Application in dye adsorption

Metallogels exhibit intrinsic and fundamental physicochemical characteristics that render them exceptionally well-suited as effective adsorbent materials. The porous network and the presence of immobilized functional moieties on the porous surface collectively facilitate direct and efficient interactions with extrinsic guest molecules selectively.[93] This phenomenon is particularly pronounced in coordination polymer-based metallogels, which inherently possess an interlinked porous architecture imbued with a substantial quantity of solvent molecules. This structural feature arises primarily due to the prevalence of weak supramolecular interactions between the gelator framework and solvent molecules, thereby engendering a dynamic and solvent-rich environment within the gel matrix. Metallogels are reported to be potential adsorbent materials, especially for water-soluble toxic organic dyes.[37] Conventional physicochemical methodologies employed for the remediation of dye-laden wastewater are

Fig. 7 Demonstration of the self-sustaining property of a metallogel (prepared using 6 mM Cu^{2+} salt with 1 : 1 Cu(II) : gelator in methanol). The weight of each Indian currency coin is 5 g.
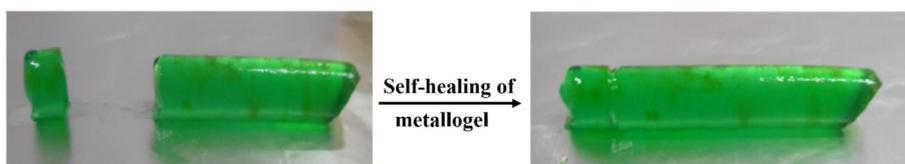

Fig. 8 Demonstration of the self-healing property of **MG1** (prepared using 12 mM Cu^{2+} salt with 1 : 1 Cu(II) : gelator in methanol).

often cost-intensive and necessitate preliminary pretreatment processes, thereby limiting their large-scale applicability. Conversely, adsorption-based strategies provide a substantially economical and efficient alternative. The adsorption efficiency of the xerogel prepared from our metallogel **MG1** was systematically evaluated for different anionic and cationic dyes such as Congo Red, Rhodamine B and Methylene Blue, representing prototypical dyes. Notably, a pronounced selectivity was observed, wherein the xerogel exhibited a markedly enhanced adsorption efficiency towards the anionic dye, Congo red. This preferential uptake underscores the intrinsic affinity of the metallogel framework for negatively charged dye species, potentially arising from synergistic electrostatic interactions and hydrogen bonding interaction from the xerogel surface, thereby reinforcing its efficacy as a highly selective and efficient adsorbent material for anionic contaminants. A time-dependent UV-visible spectroscopic analysis (Fig. 9) of a solution of Congo Red dye (5×10^{-5} M) incubated with 5 mg of xerogel revealed a bathochromic shift in the absorption maxima for the dye from 485 nm to 505 nm, which is indicative of molecular interactions between the dye and the metallogel matrix. Over an extended incubation period, a progressive attenuation in the absorption intensity was observed, concomitant with a visible bleaching of the orange coloration of the dye solution, which became increasingly pronounced after approximately 12 h, thus affirming the successful adsorption of Congo Red by the metallogel. Conversely, the presence of protonated pyridyl moieties of the OEG-functionalized terpyridyl-based gelator induced a pronounced electrostatic repulsion against cationic dyes, thereby significantly impeding their diffusion onto the adsorbent surface.[94]

The adsorbed amount of dye by the metallogel (**MG1**) was calculated using the following equation.[95]

$$Q_{eq} = \frac{(C_0 - C_{eq})V}{m}$$

where Q_{eq} (mg g^{-1}) is the amount of adsorbed dye by the metallogels, C_0 (mg L^{-1}) is the initial concentration of the dyes, C_{eq} (mg L^{-1}) is the equilibrium concentration of the dyes

in water, V (L) is the volume of the dye solution, and m (g) is the mass of the metallogels used in this adsorption experiment. From the above equation, it was calculated that 1 g of metallogel (xerogel) can adsorb 96 mg of Congo Red over a period of 8 h, demonstrating a satisfactory adsorption efficiency in line with comparable reported systems.[38,39]

Application as a reusable catalyst

The copper(I)-catalyzed azide–alkyne cycloaddition (CuAAC) reaction holds significant importance to synthesize substituted triazoles. Due to the diverse bioactivities of the triazole-based compounds, they have extensive applications in medicinal chemistry.[96,97] To explore the catalytic potential of **MG1**, both the gel-based material and xerogel (**Xel-G1**) were evaluated as catalysts, with systematic optimization of the reaction parameters, including solvent and temperature. The active Cu(I) species was generated *in situ* by reduction of the Cu(II) centre of the metallogel in the presence of an appropriate reducing agent such as sodium ascorbate. The regioselective formation of 1,4-disubstituted 1,2,3-triazole derivatives proceeds through a Huisgen 1,3-dipolar cycloaddition between organic azides and terminal alkynes, catalyzed by Cu(I) species (Scheme 2). Initially, the metallogel prepared with a 1 : 1 metal to gelator ratio was employed in the model cycloaddition reaction between benzyl azide and phenylacetylene at room temperature (28 °C) and 50 °C, yielding 1-benzyl-4-phenyltriazole in 78–82% yield (entries 2 and 3, Table S2). Upon completion, filtration of the reaction mixture revealed complete dissolution of the gel, indicating the breakdown of the gel matrix under the reaction conditions. Subsequently, xerogels were investigated for their catalytic performance (entries 4–12, Table S2). Xerogels (**Xel-G1**) were prepared by extensive drying of the freshly synthesized metallogels and subsequently employed in CuAAC reactions. Remarkably, when the reaction was conducted using **Xel-G1** at 50 °C under identical conditions, a notable improvement in conversion efficiency was observed. Moreover, the xerogel materials proved to be easily recoverable by simple filtration of the reaction mixture (Fig. S25). Initially, 0.04 mmol of Cu(I) as a xerogel and 1 mmol substrates were
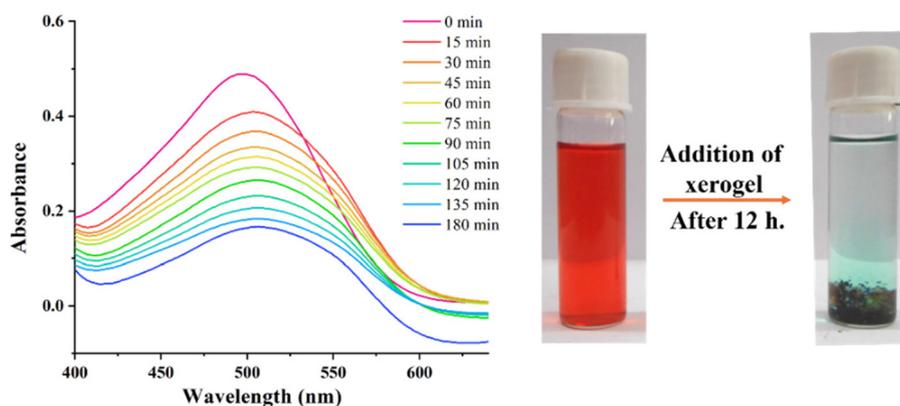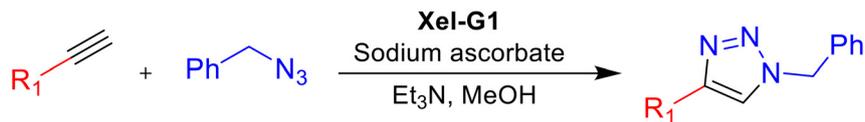

Fig. 9 Changes in the UV-visible spectra of Congo Red solution after the addition of xerogel at 15 min time intervals.

Scheme 2 A schematic illustration of the Cu(ɪ)-catalyzed azide–alkyne cycloaddition (CuAAC) affording 1,4-disubstituted 1,2,3-triazoles under mild conditions using the xerogel as a heterogeneous catalyst.

utilized for catalytic studies. However, reducing the amount of xerogel Cu(ɪ) catalyst, the yield in the CuAAC reaction is not very affected. Additionally, the xerogel with a 1 : 1 Cu/gelator ratio exhibited the highest catalytic efficiency at 50 °C, underscoring its reusability and effectiveness in CuAAC reaction (Table S3). To further refine the process, the catalyst was tested under various reaction conditions to show its applicability

Table 1 Substrate scope for the synthesis of various 1,4-disubstituted triazole derivatives using the xerogel[a]

Entry	R$_1$	mmol[b]	Yield[c] (%)
1		0.04	92
2		0.01	90
3	NC	0.003	91
4	Fe	0.005	90
5		0.006	91
6		0.02	92
7	Ph	0.001	85
8	B, F F	0.001	88
9	H$_2$N	0.001	90
10		0.01	91
11		0.01	90

[a] 1 mmol of azide and 1 mmol of phenyl acetylene. [b] Catalyst loading (mmol of Cu) was determined based on the molar quantity of Cu(ɪɪ) added (as precursor) to make the xerogel. [c] Isolated yield. The reaction temperature is 50 °C.

across a wide range of solvents, including neat conditions with minimal impact on yield as shown in Table 1.

To further investigate the scope of the catalytic reaction under the optimized conditions, we explored the cycloaddition of various alkynes with a diverse range of substrates containing electron-withdrawing (–CN) and electron-donating (–Me, –OMe) functional groups. The corresponding 1,4-disubstituted triazoles were successfully isolated in moderate to excellent yields (Table 1). After establishing 50 °C as the optimal reaction temperature, all subsequent studies were conducted under these conditions. Monitoring of the reactions involving electron-withdrawing substrates indicated that maximal yields were achieved within 2 hours (entries 3 and 5; Table 1), consistent with the enhanced electrophilicity of alkynes imparted by electron-withdrawing groups, which accelerates the reaction kinetics and improves efficiency. Conversely, electron-donating substrates, such as methoxy (–OMe) groups, required an extended reaction time of 6 hours to achieve maximum yields, a trend consistently observed for most cases (entry 2; Table 1). Furthermore, reducing the catalyst concentration from the optimized value still yielded better conversions for electron-deficient substrates, highlighting their inherent reactivity under these conditions. Additionally, it was observed that alkyl-substituted counterparts also provided comparable yields similar to the aryl alkyne substitution. The synthesized triazole derivatives were further characterized using mass spectrometry, confirming their structural integrity (Fig. S13a–j). The exclusive 1,4-disubstituted regioselectivity of the Cu-catalyzed reaction was further corroborated by ^{13}C NMR analysis, wherein the characteristic C$_5$ carbon signal of the triazole core appeared at 119.4 ppm, in agreement with previously reported literature values (Fig. S9).[98]

This heterogeneous catalysis of azide–alkyne 1,3-dipolar cycloaddition reactions offers significant advantages over homogeneous catalysis, particularly with respect to catalyst reusability and operational stability. One of the most noteworthy attributes of the xerogel was its exceptional recyclability as a catalytic material. The Cu(ɪ)–xerogel catalyst moreover exhibited remarkable stability against oxygen and moisture, allowing it to be stored for an extended period without degradation. To further assess its durability, the xerogel containing Cu(ɪ) was exposed to ambient atmospheric conditions for 72 hours before being tested for catalytic activity. When applied to the reaction between benzyl azide and phenyl acetylene, it retained an impressive yield of 81%, demonstrating its robustness under prolonged exposure. A particularly striking feature of the 1 : 1 xerogel catalyst was its ability to maintain catalytic

efficiency over multiple reaction cycles (Fig. S25). Even after five consecutive cycles, the xerogel retained its activity with minimal loss of reactivity, highlighting its exceptional recyclability. The xerogel was successfully recovered *via* filtration and reused in four subsequent cycles without any appreciable decline in performance. However, after five catalytic cycles, a gradual decrease in activity was observed, with the yield declining from approximately 90% to 67%, further emphasizing its practical applicability as a recyclable catalytic system.

3. Conclusions

In summary, we have successfully designed and synthesized an oligo(ethylene glycol)-bridged bis-terpyridyl ligand by strategically incorporating multiple supramolecular interaction sites to facilitate coordination-driven self-assembly. The synthesized gelator demonstrated a remarkable ability to form stable metallogels exclusively with Cu^{2+} ions, independent of the nature of the anion, across a range of solvent environments. Notably, the gelation behavior was observed predominantly in polar solvents, whereas no gel formation was detected in non-polar media, highlighting the solvent-dependent self-assembly characteristics. One of the most intriguing features of the metallogel was its multi-stimuli responsive nature, wherein mechanical agitation or the application of shear force resulted in the breakdown of the gel network, followed by rapid self-recovery within a few minutes. This reversible sol–gel transition could be cycled multiple times, demonstrating its dynamic adaptability. Additionally, the metallogel exhibited self-healing properties, further reinforcing its structural resilience and suitability for smart material applications. The value of G' is considerably higher in the gel state – approximately 1000 Pa in methanol – indicating a gel of moderate strength and supporting the presence of softer metal–ligand coordinative interactions. Beyond its mechanical robustness, the gel also showcased promising adsorption capabilities, particularly in the removal of anionic dyes from aqueous solutions, emphasizing its potential utility in environmental remediation. Furthermore, the xerogel, derived from the metallogel through solvent removal, demonstrated excellent catalytic efficiency in the Cu(ɪ)-catalyzed azide–alkyne cycloaddition (CuAAC) reaction, producing regioselective 1,4-disubstituted 1,2,3-triazoles. The xerogel catalyst exhibited high stability, retained its catalytic activity even after multiple cycles, and remained structurally intact under ambient conditions. Collectively, these findings emphasize the multifunctional nature of the synthesized metallogel, integrating stimuli-responsive gelation, self-healing ability, dye adsorption properties, and catalytic efficiency into a single supramolecular system. Given these exceptional properties of this Cu(ɪɪ)–metallogel system, further design to achieve multifunctional metallogels with low molecular weight gelators that exhibit potential applications in developing smart materials, environmental remediation, and sustainable catalysis are underway in our laboratory.

4. Experimental

Syntheses

Synthesis of 4′-(4-methylphenyl)-2,2′:6′,2″-terpyridine (tpy) (1). 8 mL of 2-acetylpyridine (71.32 mmol) was added to a solution of 4.2 mL of 4-methyl benzaldehyde (35.95 mmol) in ethanol followed by the addition of 4.0 g NaOH (71.32 mmol) and 80 mL of aqueous NH_3 (6.5 mmol); the solution was then stirred overnight at room temperature, after which an orange suspension appeared. The solid was collected by filtration and washed with EtOH (3 × 60 mL). Then the crude solid product was recrystallized by cooling the hot supersaturated ethanolic solution.[99] Yield: 2.50 g (60%). ^1H NMR (CDCl₃, 400 MHz, ppm): δ, 2.44 (s, methyl 3H), 7.31–7.37 (m, 4H), 7.82 (d, J = 8 Hz, pyridyl 2H), 7.88 (m, pyridyl 2H), 8.68 (d, J = 8 Hz, pyridyl 2H), 8.73 (d, J = 4 Hz, pyridyl 2H), 8.74 (s, pyridyl 2H); $^{13}C\{^1H\}$ NMR (CDCl₃, 100 MHz, ppm): δ 21.5, 118.8, 121.6, 123.9, 127.3, 129.8, 135.6, 137.1, 139.3, 149.2, 150.3, 155.9, 156.5.

Synthesis of 4′-(4-bromomethylphenyl)-2,2′:6′,2″-terpyridine (Brtpy) (2). A mixture of 4′-(4-methylphenyl)-2,2′:6′,2″-terpyridine (4.05 g, 12.43 mmol), *N*-bromosuccinimide (NBS, 2.42 g, 13.61 mmol) and azobis(isobutyroniltrile) (AIBN, 163 mg, 0.99 mmol) in dry CCl₄ (40 ml) was refluxed for 3 h. The warm reaction mixture was filtered to remove succinimide and the solvent was evaporated under reduced pressure.[100] The crude product was recrystallized from EtOH to give a pale-yellow solid. Yield: 1.10 g (84%). ^1H NMR (CDCl₃, 400 MHz, ppm): δ, 4.57 (s, methylene 2H), 7.40 (t, J = 8 Hz, 2H), 7.55 (d, J = 8 Hz, 2H), 7.93 (m, pyridyl 4H), 8.71 (d, J = 8 Hz, pyridyl 2H), 8.75 (d, J = 4 Hz, pyridyl 2H), 8.79 (s, pyridyl 2H); $^{13}C\{^1H\}$ NMR (CDCl₃, 100 MHz, ppm): δ, 33.2, 119.0, 121.6, 124.1, 127.9, 129.8, 137.1, 138.7, 138.8, 149.3, 149.7, 156.1, 156.3.

Synthesis of Gelator L1 (Tpy-OEG₃₀₀-Tpy). To an oven dried Schlenk flask, a solution of oligoethylene glycol (OEG₃₀₀) (1.0 g, 2.48 mmol) in THF (8 mL) at 25 °C, NaH (60% in paraffin, 250 mg, 520.0 mmol) was added slowly and the resulting mixture was stirred for 30 min at room temperature. Then compound **2** (5.12 g, 6.20 mmol) was added and the resulting mixture was stirred overnight. After quenching the reaction mixture with H_2O (20 ml), it was extracted with EtOAc (4 × 30 mL), and the combined organic phases were dried by using anhydrous $MgSO_4$. The solvent was evaporated by rotary evaporation. The residue was then purified by flash chromatography on silica gel (*n*-hexane/EtOAc = 1 : 1) to get compound **L1** as a clear oil. Yield: 7.65 g (76%). ^1H NMR (CDCl₃, 400 MHz): δ, 4.66 (s, methylene 2H), 3.64–3.71 (m, OEG-chain-H), 7.38 (t, J = 8 Hz, 2H), 7.49 (d, J = 8 Hz, 2H), 7.92 (m, pyridyl 4H), 8.69 (d, J = 8 Hz, pyridyl 2H), 8.74 (d, J = 4 Hz, pyridyl 2H), 8.79 (s, pyridyl 2H); $^{13}C\{^1H\}$ NMR (CDCl₃, 100 MHz): δ, 33.2, 119.0, 121.6, 124.1, 127.9, 129.8, 137.1, 138.7, 138.8, 149.3, 149.7, 156.1, 156.3. MALDI-TOF MS (positive mode): m/z = 882.450 $[M + H]^+$ (x = 5); 926.525 $[M + H]^+$ (x = 6); 970.602 $[M + H]^+$ (x = 7); 1014.678 $[M + H]^+$ (x = 8); 1058.755 $[M + H]^+$ (x = 9); 1102.833 $[M + H]^+$ (x = 10); x = units of $-CH_2CH_2O-$ in OEG₃₀₀.

Author contributions

PP and UG contributed to the experimental work, data collection, and overall investigation. AS was involved in data analysis and contributed to scientific discussions. SKP performed data validation and formal analysis, and was responsible for drafting and reviewing the manuscript.

Conflicts of interest

The authors declare no conflicts of interest.

Data availability

Supplementary information: synthesis procedures of all compounds, along with their corresponding characterization data, general methods and instrument details. Relevant literature references supporting these methods are also included. See DOI: https://doi.org/10.1039/d5dt01843a.

Acknowledgements

References

1 Q. Zhang, Y. X. Deng, H. X. Luo, C. Y. Shi, G. M. Geise, B. L. Feringa, H. Tian and D. H. Qu, *J. Am. Chem. Soc.*, 2019, **141**, 12804–12814.

2 P. Dastidar, S. Ganguly and K. Sarkar, *Chem. – Asian J.*, 2016, **11**, 2484–2498.

3 K. J. Skilling, F. Citossi, T. D. Bradshaw, M. Ashford, B. Kellam and M. Marlow, *Soft Matter*, 2014, **10**, 237–256.

4 X. M. Li, J. Y. Li, Y. A. Gao, Y. Kuang, J. F. Shi and B. Xu, *J. Am. Chem. Soc.*, 2010, **132**, 17707–17709.

5 A. Vintiloiu and J.-C. Leroux, *J. Controlled Release*, 2008, **125**, 179–192.

6 P. Biswas and P. Dastidar, *Inorg. Chem.*, 2021, **60**, 3218–3231.

7 J. H. Jung, M. Park and S. Shinkai, *Chem. Soc. Rev.*, 2010, **39**, 4286–4302.

8 B. Escuder, F. Rodriguez-Llansola and J. F. Miravet, *New J. Chem.*, 2010, **34**, 1044–1054.

9 V. K. Praveen, C. Ranjith and N. Armaroli, *Angew. Chem., Int. Ed.*, 2014, **53**, 365–368.

10 S. S. Babu, V. K. Praveen, K. K. Kartha, S. Mahesh and A. Ajayaghosh, *Chem. – Asian J.*, 2014, **9**, 1830–1840.

11 A. Ajayaghosh, V. K. Praveen, C. Vijayakumar and S. J. George, *Angew. Chem., Int. Ed.*, 2007, **46**, 6260–6265.

12 P. Duan, N. Yanai, H. Nagatomi and N. Kimizuka, *J. Am. Chem. Soc.*, 2015, **137**, 1887–1894.

13 S. S. Babu, S. Prasanthkumar and A. Ajayaghosh, *Angew. Chem., Int. Ed.*, 2012, **51**, 1766–1776.

14 S. Sedghiniya, J. Soleimannejad and A. J. Blake, *Mater. Today Commun.*, 2021, **27**, 102448.

15 L. A. Estroff and A. D. Hamilton, *Chem. Rev.*, 2004, **104**, 1201–1218.

16 S. S. Babu, V. K. Praveen and A. Ajayaghosh, *Chem. Rev.*, 2014, **114**, 1973–2129.

17 R. G. Weiss, *J. Am. Chem. Soc.*, 2014, **136**, 7519–7530.

18 C. Tomasini and N. Castellucci, *Chem. Soc. Rev.*, 2013, **42**, 156–172.

19 L. E. Buerkle and S. J. Rowan, *Chem. Soc. Rev.*, 2012, **41**, 6089–6102.

20 R. G. Weiss and P. Terech, *Molecular Gels: Materials with Self-Assembled Fibrillar Networks*, Springer, Dordrecht, The Netherlands, 2006, pp. 1–978.

21 H. Kumari, S. E. Armitage, S. R. Kline, K. K. Damodaran, S. R. Kennedy, J. L. Atwood and J. W. Steed, *Soft Matter*, 2015, **11**, 8471–8478.

22 S. Banerjee, V. M. Vidya, A. J. Savyasachi and U. Maitra, *J. Mater. Chem.*, 2011, **21**, 14693–14705.

23 L. Meazza, J. A. Foster, K. Fucke, P. Metrangolo, G. Resnati and J. W. Steed, *Nat. Chem.*, 2013, **5**, 42–47.

24 A. Bertolani, L. Pirrie, L. Stefan, N. Houbenov, J. S. Haataja, L. Catalano, G. Terraneo, G. Giancane, L. Valli, R. Milani, O. Ikkala, G. Resnati and P. Metrangolo, *Nat. Commun.*, 2015, **6**, 7574–7582.

25 P. Bertsch, M. Diba, D. J. Mooney and S. C. G. Leeuwenburgh, *Chem. Rev.*, 2023, **123**, 834–873.

26 M. D. Segarra-Maset, V. J. Nebot, J. F. Miravet and B. Escuder, *Chem. Soc. Rev.*, 2013, **42**, 7086–7098.

27 X. Yu, L. Chen, M. Zhang and T. Yi, *Chem. Soc. Rev.*, 2014, **43**, 5346–5371.

28 S. Basak, J. Nanda and A. Banerjee, *Chem. Commun.*, 2014, **50**, 2356–2359.

29 G. Liu, J. Sheng, W. L. Teo, G. Yang, H. Wu, Y. Li and Y. Zhao, *J. Am. Chem. Soc.*, 2018, **140**, 16275–16283.

30 S. D. Kurbah and R. A. Lal, *Inorg. Chem. Commun.*, 2020, **111**, 107642.

31 B. N. Ghosh, S. Bhowmik, P. Mal and K. Rissanen, *Chem. Commun.*, 2014, **50**, 734–736.

32 S. Lin, Z. Song, G. Che, A. Ren, P. Li, C. Liu and J. Zhang, *Microporous Mesoporous Mater.*, 2014, **193**, 27–34.

33 J. Fernández, J. Kiwi, C. Lizama, J. Freer, J. Baeza and H. D. Mansilla, *J. Photochem. Photobiol., A*, 2002, **151**, 213–219.

34 D. Mahanta, G. Madras, S. Radhakrishnan and S. Patil, *J. Phys. Chem. B*, 2008, **112**, 10153–10157.

35 F. Y. Yi, W. Zhu, S. Dang, J. P. Li, D. Wu, Y. H. Li and Z. M. Sun, *Chem. Commun.*, 2015, **51**, 3336–3339.

36 S. Deng, H. Xu, X. Jiang and J. Yin, *Macromolecules*, 2013, **46**, 2399–2406.

37 N. Alam and D. Sarma, *ACS Omega*, 2020, **5**, 17356–17366.

38 C. K. Karan and M. Bhattacharjee, *ACS Appl. Mater. Interfaces*, 2016, **8**, 5526–5535.

39 M. Dutta, K. Karan and M. Bhattacharjee, *ChemistrySelect*, 2022, 7, e202203214.

40 M. O. Guler and S. I. Stupp, *J. Am. Chem. Soc.*, 2007, **129**, 12082–12083.

41 T. Tu, W. Assenmacher, H. Peterlik, R. Weisbarth, M. Nieger and K. H. Dötz, *Angew. Chem., Int. Ed.*, 2007, **46**, 6368–6371.

42 J. Zhang, X. Wang, L. He, L. Chen, C. Y. Su and S. L. James, *New J. Chem.*, 2009, **33**, 1070–1075.

43 F. Shi, Q. Zhang, D. Li and Y. Deng, *Chem. – Eur. J.*, 2005, **11**, 5279–5288.

44 D. D. Díaz, D. Kühbeck and R. J. Koopmans, *Chem. Soc. Rev.*, 2011, **40**, 427–448.

45 S. Bera and D. Haldar, *J. Mater. Chem. A*, 2016, **4**, 6933–6939.

46 Y. Hisamatsu, S. Banerjee, M. B. Avinash, T. Govindaraju and C. Schmuck, *Angew. Chem., Int. Ed.*, 2013, **52**, 12550–12554.

47 P. Sutar and T. K. Maji, *Chem. Commun.*, 2016, **52**, 8055–8074.

48 G. Picci, C. Caltagirone, A. Garau, V. Lippolis, J. Milia and J. W. Steed, *Coord. Chem. Rev.*, 2023, **492**, 215225.

49 N. Alam, S. Mondal and D. Sarma, *Coord. Chem. Rev.*, 2024, **504**, 215673.

50 A. Biswas, S. Mukhopadhyay, R. S. Singh, A. Kumar, N. K. Rana, B. Koch and D. S. Pandey, *ACS Omega*, 2018, **3**, 5417–5425.

51 J. Shukla, Y. Kumar, M. K. Dixit, C. Mahendar, V. K. Sharma, A. Kalam and M. Dubey, *Chem. – Asian J.*, 2020, **15**, 3020–3028.

52 Y. Zhang, Q. F. Zhou, G. F. Huo, G. Q. Yin, X. L. Zhao, B. Jiang, H. Tan, X. Li and H. B. Yang, *Inorg. Chem.*, 2018, **57**, 3516–3520.

53 A. Y. Tam and V. W. Yam, *Chem. Soc. Rev.*, 2013, **42**, 1540–1567.

54 J. Zhang and C.-Y. Su, *Coord. Chem. Rev.*, 2013, **257**, 1373–1140.

55 J. Zhang, X. Wang, L. He, L. Chen, C. Y. Su and S. L. James, *New J. Chem.*, 2009, **33**, 1070–1075.

56 B. Dey, S. Sadhu, D. Saha, S. J. Behera, A. Kundu, R. R. Kumar, S. K. Yatirajula and J. Rath, *Inorg. Chem. Commun.*, 2025, **178**, 114571.

57 I. Pal, S. Ghosh, D. Saha, S. Majumdar, S. K. Yatirajula, P. P. Ray and B. Dey, *Inorg. Chem.*, 2025, **64**, 5971–5985.

58 B. Dey, D. Saha, B. Bhattacharjee, S. Sadhu, R. Dey, S. K. Yatirajula, A. Chakrovorty and A. Samadder, *Langmuir*, 2025, **41**, 21107–21124.

59 D. D. Díaz, D. Kühbeck and R. J. Koopmans, *Chem. Soc. Rev.*, 2011, **40**, 427–448.

60 T. Tu, W. Fang, X. Bao, X. Li and K. H. Dötz, *Angew. Chem., Int. Ed.*, 2011, **50**, 6601–6605.

61 C. Butler, S. Goetz, C. M. Fitchett, P. E. Kruger and T. Gunnlaugsson, *Inorg. Chem.*, 2011, **50**, 2723–2725.

62 M. Dubey, A. Kumar, K. R. Gupta and D. S. Pandey, *Chem. Commun.*, 2014, **50**, 8144–8147.

63 R. Kuosmanen, K. Rissanen and E. Sievänen, *Chem. Soc. Rev.*, 2020, **49**, 1977–1998.

64 L. Zang, C. Luan, X. Tang, J. Lu and Y. Zhao, *Dyes Pigm.*, 2021, **196**, 109751.

65 F. Houard, A. Olivier, G. Cucinotta, O. Galangau, M. Gautier, F. Camerel, T. Guizouarn, T. Roisnel, B. Le Guennic, M. Ozerov, Y. Suffren, G. Calvez, C. Daiguebonne, O. Guillou, F. Artzner, M. Mannini and K. Bernot, *J. Mater. Chem. C*, 2024, **12**, 3228–3237.

66 H. Wu, J. Zheng, A. L. Kjøniksen, W. Wang, Y. Zhang and J. Ma, *Adv. Mater.*, 2019, **31**, 1903062.

67 P. J. M. Stals, J. F. Haveman, R. Martín-Rapún, C. F. C. Fitié, A. R. A. Palmans and E. W. Meijer, *J. Mater. Chem.*, 2009, **19**, 124–130.

68 W. Fang, C. Liu, J. Chen, Z. Lu, Z. M. Li, X. Baoc and T. Tu, *Chem. Commun.*, 2015, **51**, 4267–4270.

69 H. Yang, A. Wang, L. Zhang, X. Zhou, G. Yang, Y. Li, Y. Zhang, B. Zhang, J. Song and Y. Feng, *New J. Chem.*, 2017, **41**, 15173–15179.

70 T. Singha Mahapatra, H. Singh, A. Maity, A. Dey, S. K. Pramanik, E. Suresh and A. Das, *J. Mater. Chem. C*, 2018, **6**, 9756–9766.

71 P. Peng, Y. Li, W. Song and X. Yu, *Colloids Surf., A*, 2020, **589**, 124439.

72 A. Biswas, S. Mukhopadhyay, R. S. Singh and D. S. Pandey, *ChemistrySelect*, 2016, **1**, 1904–1909.

73 B. C. Roy and T. S. Mahapatra, *Soft Matter*, 2023, **19**, 1854–1872.

74 Y. Li, J. Guo, B. Dai, L. Geng, F. Shen, Y. Zhang and X. Yu, *J. Colloid Interface Sci.*, 2018, **521**, 190–196.

75 T. Zhao, S. Chen, K. Kang, J. Ren and X. Yu, *Langmuir*, 2022, **38**, 1398–1405.

76 R. Wang, M. Geven, P. J. Dijkstra, P. Martens and M. Karperien, *Soft Matter*, 2014, **10**, 7328–7336.

77 P. Peng, Y. Li, W. Song and X. Yu, *Colloids Surf., A*, 2020, **589**, 124439.

78 H. R. Khavasi and E. Jelokhani, *J. Mater. Chem. A*, 2019, **7**, 6638–6643.

79 L. Arnedo-Sánchez, Nonappa, S. Bhowmik, S. Hietala, R. Puttreddy, M. Lahtinen, L. De Cola and K. Rissanen, *Dalton Trans.*, 2017, **46**, 7309–7316.

80 E. Hendrickx, K. Clays and A. Persoons, *Acc. Chem. Res.*, 1998, **31**, 675–684.

81 F. Krohnke, *Synthesis*, 1976, 1–24.

82 S. Lee, Y. Park, K. R. Wee, H. Son, D. W. Cho, C. Pac, W. Choi and S. O. Kang, *Org. Lett.*, 2010, **12**, 460–463.

83 S. Chandrasekhar, C. Narsihmulu, S. S. Sultana and N. R. Reddy, *Org. Lett.*, 2002, **4**, 4399–4401.

84 K. Czerwińska, B. Machura, S. Kula, S. Krompiec, K. Erfurt, C. Roma-Rodrigues, A. R. Fernandes, L. S. Shul'Pina, N. S. Ikonnikov and G. B. Shul'Pin, *Dalton Trans.*, 2017, **46**, 9591–9604.

85 K. Choroba, B. Machura, K. Erfurt, A. R. Casimiro, S. Cordeiro, P. V. Baptista and A. R. Fernandes, *J. Med. Chem.*, 2024, **67**, 5813–5836.

86 T. Todorovic, S. Grubišic, M. Pregelj, M. Jagodič, S. Misirlic-Denčic, M. Dulovic, I. Markovic, O. Klisuric, A. Maleševic, D. Mitic, K. And Strok Signelkovic and N. Filipović, *Eur. J. Inorg. Chem.*, 2015, 3921–3931.

87 M. Martinez-Calvo, O. Kotova, M. E. Mobius, A. P. Bell, T. McCabe, J. J. Boland and T. Gunnlaugsson, *J. Am. Chem. Soc.*, 2015, **137**, 1983–1992.

88 A. J. A. Baker, E. J. Galindo, J. D. Angelos, D. K. Salazar, S. M. Sterritt, A. M. Willis and M. S. Tartis, *Data Brief*, 2023, **48**, 109114.

89 X. Yan, D. Xu, X. Chi, J. Chen, S. Dong, X. Ding, Y. Yu and F. Huang, *Adv. Mater.*, 2012, **24**, 362–369.

90 S. Samai and K. Biradha, *Chem. Mater.*, 2012, **24**, 1165–1173.

91 S. Saha, J. Bachl, T. Kundu, D. Diaz Diaz and R. Banerjee, *Chem. Commun.*, 2014, **50**, 3004–3006.

92 P. Bertsch, M. Diba, D. J. Mooney and S. C. G. Leeuwenburgh, *Chem. Rev.*, 2023, **123**, 834–873.

93 M. O. Guler and S. I. Stupp, *J. Am. Chem. Soc.*, 2007, **129**, 12082–12083.

94 M. A. Usman and A. Y. Khan, *J. Hazard. Mater.*, 2022, **428**, 128238.

95 L. Liang and D. Astruc, *Coord. Chem. Rev.*, 2011, **255**, 2933–2945.

96 C.-H. Wong and S. C. Zimmerman, *Chem. Commun.*, 2013, **49**, 1679–1695.

97 V. V. Rostovtsev, L. G. Green, V. V. Fokin and K. B. Sharpless, *Angew. Chem., Int. Ed.*, 2002, **41**, 2596–2599.

98 X. Creary, A. Anderson, C. Brophy, F. Crowell and Z. Funk, *J. Org. Chem.*, 2012, **77**, 8756–8761.

99 T. N. Francisco, H. M. T. Albuquerque and A. M. S. Silva, *Chem. – Eur. J.*, 2024, **30**(47), 1–25.

100 P. K. Pramanick, Z. L. Hou and B. Yao, *Tetrahedron*, 2017, **73**, 7105–7114.